nature nanotechnology

SUPPLEMENTARY INFORMATION

DOI: 10.1038/NNANO.2012.162

# Selective Molecular Sieving Through Porous Graphene

Steven P. Koenig, Luda Wang, John Pellegrino, and J. Scott Bunch*

*email: jbunch@colorado.edu

**Supplementary Information:**

## 1. Raman Spectrum of Graphene Flakes

Raman spectroscopy was used to support our conclusion that a small number of pores exist in the graphene flakes. The D-peak (1360 $cm^{-1}$ wavenumber) is associated with defects in the graphene lattice. Figure S1 shows the Raman spectrum of the graphene flakes used in this study. Figure S1a shows the Raman spectrum of membrane 'Bi- 3.4 Å' presented in the main text. This spectrum was taken "before-etching" but is identical to the "after-etching" Raman spectrum. Both spectrums show no D-peak. Figure S1b shows the ratio of the graphene G-peak to the silicon peak areas for the flake presented in this study (the red closed square) and a nearby flake which contained mono- and bi-layer portions (the black open circle for mono-layer and red open square for bi-layer). This follows the work by Koh et al to confirm we had bilayer graphene[1]. Figure S1c shows the Raman spectrum for membrane 'Bi- 4.9 Å' presented in the main text "before-etching" showing the characteristic 2D peak shape of bilayer graphene. Figure S1d shows the Raman spectrum of the two monolayer membranes presented in the supplementary information, 'Mono-3.4 Å', from Figure S5, (upper red curve) and 'Mono-5 Å', presented in Figure S6 (lower black curve). Both spectrums presented in Figure S1d were taken "after-etching". 'Mono- 3.4 Å' showed similar $H_2$ leaking behavior as membrane 'Bi- 3.4 Å' presented in the main text. No spatial variation was seen in the Raman spectrum of these flakes after-etching. There has been no D-peak observed in etched monolayer samples that showed gas selectivity and we have observed a D-peak in bilayer samples showing selectivity but future work will be needed to correlate the D-peak with pore density since the top layer of bilayer graphene will likely etch before the bottom layer does to open up pores.

## 2. Etching Pores in Graphene Membranes

In order to etch the graphene membranes, we first pressurized them with pure $H_2$

up to 200 kPa (gauge pressure) above ambient pressure. After the microcavity reached equilibrium we removed it from the pressure chamber and measured the deflection using atomic force microscopy (AFM). We then did a series of short UV etches (30 s) followed by AFM scans between each etching step to see if the leak rate increased significantly. When pore(s) were created that were selective to allow the $H_2$ to pass through, but not allow the molecules in the air to pass, the deflection would rapidly decrease and become negative, consistent with a vacuum inside the microcavity. For the case of the 'Bi- 3.4 Å' membrane in the main text, this etching took 75 min (150, 30 s etching steps). Each etch step took about 5 min to complete. Once the sample was out of the pressure chamber for over an hour during the etching process, and the deflection had decreased 20 nm, we then returned the sample to the pressure chamber overnight to allow the pressure inside the microchamber to once again reach 200 kPa. The etching process was then continued the next day. For membrane 'Bi- 4.9 Å' in the main text, the total etching time was 15 min using 1 min etching steps. From the etching experiments it was noted that longer etch steps required significantly less total etching time.

Since we conclude that there are only a small number of sub-nanometer pores in the 5 μm membranes, direct imaging of these pores is not possible. For classical effusion of gas out of the microcavity, the number of molecules in the microcavity is given by:

$$n = n_0 e^{-\frac{A}{V}\sqrt{\frac{k_b T}{2\pi m}}t} \qquad (S1)$$

where $n_0$ is the initial number of molecules, $A$ is the area of the hole, $V$ is the volume of the container, $k_b$ is Boltzman's constant, $T$ is temperature, $t$ is time, and $m$ is the molecular mass of the gas undergoing effusion[2,3]. For a 3 Å diameter circular pore, and 100 kPa $H_2$ pressure, the leak rate is ~$10^{-20}$ mol·s$^{-1}$·Pa$^{-1}$ which should be fast enough to experimentally measure by our technique and on the order of the leak rates presented here.

In order to visualize pores created by the UV induced oxidative etching reported in the main text, one membrane was over-etched to create much larger pores so we could image the pore formation and distribution with AFM. Figure S2 shows a monolayer membrane that was over-etched (22 min total with 1 min etching steps) in order to visualize the pore growth. Fig S2a shows the 500 nm x 500 nm AFM scan over the suspended region of the over-etched graphene membrane. This membrane was not

selective to any of the gas species tested and the leak rates were too fast to measure. The results of the pore size distribution seen in Fig. S2b and Fig. S2c are comparable to previous oxidative etching of graphene and graphite (see references 14,15, and 19 from them main text).

## 3. Calculating the Pressure Normalized Leak Rate from Deflection versus *t* Data

The deformation of the membrane can be described using Hencky's (1915) solution for a pressurized clamped circular elastic membrane with a pressure difference of $\Delta p$ across it:

$$\Delta p = K(\nu)(Ew\delta^3)/a^4 \qquad (S2)$$

where $E$ is the Young's modulus, $\nu$ is the Poisson's ratio, $w$ is the membrane thickness, and $K(\nu)$ is a coefficient that depends only on $\nu$ [4]. For the case of graphene, we take $E$=1TPa and $\nu$=0.16, therefore $K(\nu=0.16)=3.09$[5]. In order to derive $dn/dt$, the leak rate of the microcavity, we start with the ideal gas law:

$$PV(\delta) = nRT \qquad (S3)$$

where $P$ is the absolute pressure inside the microcavity, $V(\delta)$ is the volume of the microcavity when the membrane is bulged with deflection $\delta$, $V(\delta)=V_o+V_b(\delta)$, $V_b(\delta)=C(\nu)\pi a^2\delta$, for graphene $C(\nu = 0.16) = 0.52$, $n$ is the number of moles of gas molecules contained in the microcavity, $R$ is the gas constant, and $T$ is temperature[5]. Substituting $(\Delta p+p_{atm})$ for $P$ and dividing both sides by $V(\delta)$, and inserting Henckey's solution for $\Delta p$ we get:

$$(K(\nu)(Ew\delta^3)/a^4 + p_{atm}) = \frac{nRT}{V_o + V_b(\delta)} \qquad (S4)$$

Now we can take the time derivative of both sides and solve for $dn/dt$ to get the flux of gas molecules out of the membrane:

$$\frac{dn}{dt} = \frac{[3K(\nu)(Ew\delta^2)/a^4 \cdot V(\delta) + P(C(\nu)\pi a^2)]}{RT} \cdot \frac{d\delta}{dt} \qquad (S5)$$

To get the $dn/dt$ (mol/s), we use the measured $d\delta/dt$, the rate of the bulge decay from the linear fit of the membrane deflection versus time data. We then normalize the leak rate by dividing the calculated $dn/dt$ by the pressure driving force for each of the gases measured to get the leak rate out of the microcavity.

## 4. Calculating the Pressure Normalized Leak Rate from Frequency versus *t* Data

A schematic of the resonance measurement is presented in Fig S3. Figure S3a shows a membrane that is exposed to a gas smaller than the pore(s) in the graphene thus able to pass through after the membrane has been initially placed in vacuum. Over time, the molecules will leak into the microcavity causing the deflection, and thus the tension, to decrease which leads to a decreasing resonant frequency. Figure S3b shows the membrane in a gas species that is larger than the pore(s) in the graphene. Since the gas is larger than the pore(s) it is blocked and the resonant frequency does not change over time. For the case of the gas being able to pass through the graphene membrane, once the pressure begins to equilibrate on both sides, the signal is lost due to significant gas damping, and it is not possible to accurately experimentally resolve the resonant frequency. This can be seen in the $CH_4$ data presented Fig S4. This data is resonant frequency curves from the $CH_4$ leak rate found in Fig 3 inlay of the main text with 80 torr initially introduced across the membrane. The black curve is the original frequency, $t$ = 0 s. The red curve is the frequency right after the pressure is introduced to the membrane, $t$ = 1 s. From the red curve you can see there is already a significant gas damping which is evident because of the lower quality factor (i.e. broader peak). The green, blue, cyan, and magenta curves correspond to $t$ = 3 s, $t$ = 5 s, $t$ = 7 s, and $t$ = 11 s, respectively. At $t$ = 13 s (orange curve) the damping is too large to discern a peak and we cannot determine what the resonant frequency is at or after this time.

The frequency of a circular membrane under tension caused by a pressure difference $\Delta p$ can be described using the following 3 equations:

$$f = \frac{2.404}{2\pi}\sqrt{\frac{S}{\rho_A a^2}} \qquad (S6)$$

$$S = \frac{\Delta p a^2}{4\delta} + S_0 \qquad (S7)$$

$$\Delta p = K(\nu)(Ew\delta^3)/a^4 + (4S_0\delta)/a^2 \qquad (S8)$$

where $f$ is the resonant frequency of the membrane, $a$ is the radius of the membrane, $S$ is the tension in the membrane due to the applied pressure and $S_0$ is the initial tension in the

membrane, and $\rho_A$ is the mass density[6]. *K(ν)* and *E* are elastic constants from Hencky's solution and *w* is the thickness of the membrane and $\delta$ is the deflection in the membrane[4]. We do not take $S_0$ to be zero in this case since the pressure difference and thus the deflection of the membrane are small compared with the case of the blister test. In order to derive the *dn/dt*, the leak rate of the microcavity we first need to solve for *S* by combining (S7) and (S8) to get:

$$S^3 - 4S^2 + 5S{S_0}^2 - 2{S_0}^3 = K(\nu)(Ewa^2\Delta p^2)/64 \qquad (S9)$$

Since *S* is larger than $S_0$ we can neglect the cubic order term of $S_0$. Now we can insert the expression for *S* into equation (S6) and solve for *Δp,* and then insert this expression for *Δp* into the ideal gas law in a similar fashion as the bulge test equation. Since the deflection of the membrane is small in this case we take *V* to be constant. After doing this and taking time derivative and solving for *dn*/*dt* we arrive at the expression:

$$\frac{dn}{dt} = \frac{V}{RT}\left[\left(\frac{(c_1\rho_A - 2c_2{\rho_A}^2a^2f^2){S_0}^2 + c_3{\rho_A}^3a^4f^4}{4K(\nu)Ew}\right)^{1/2} + \frac{c_3{\rho_A}^3a^4f^4 - c_2S_0{\rho_A}^2a^2f^2}{\left(K(\nu)Ew((c_1\rho_A - 2c_2{\rho_A}^2a^2f^2){S_0}^2 + c_3{\rho_A}^3a^4f^4)\right)^{1/2}}\right]\frac{df}{dt} \qquad (S10)$$

where $c_1$, $c_2$, and $c_3$ are constants equal to $8.74\text{x}10^3$, $2.39\text{x}10^4$, and $8.16\text{x}10^4$, respectively. To get *dn/dt (mol/s)* we can use *df/dt*, the rate of the frequency decay from the linear fit of the membrane frequency versus time data. We then normalize the leak rate by dividing the calculated *dn/dt* by the pressure driving force for each of the gases measured to get the leak rate (normalized *dn/dt*) into the graphene-sealed microcavity.

## 5. Additional Membranes Measured

Three additional membranes where measured, two monolayer and two bilayer samples. The monolayer sample in Fig. S5 ('Mono- 3.4 Å') shows similar behaviour as seen in 'Bi- 3.4 Å' of the main text. This monolayer sample was filled with 150 kPa above ambient pressure with pure $H_2$. The pore was not stable and additional measurements could not be taken. The second monolayer sample shown in Fig. S6 was measured using the mechanical resonance scheme presented in the main text. This membrane showed a similar pore instability as the previous sample. The order of the leak rate measurements taken on this membrane were $N_2$ (black), $H_2$ (red), $CO_2$ (green), and

$CH_4$ (blue). Next, $N_2$ was measured a second time (cyan) showing a drastic increase in the $N_2$ leak rate. After the repeat of the $N_2$ data, we then introduced $SF_6$, and the results show that the membrane is slowly allowing $SF_6$ to permeate indicating that this pore is larger but similar in size to $SF_6$ (4.9Å)[7]. We attribute this increase in $N_2$ leak rate to etching of the pore during the resonance measurement.

Two additional bilayer membranes from the same graphene flake found in Fig. 1 (containing membrane 'Bi- 3.4 Å') of the main text are shown in Fig. S7. Figure S7a is a membrane that has larger pores than that of the sample presented in the main text. The membrane in Fig. S7a was damaged before $CH_4$ leak rate data could be taken. Fig S7b is the sample presented in the main text, and Fig. S7c shows the leak rate of a membrane that showed molecular sieving of $H_2$ versus $CO_2$ and larger molecules (Ar, $N_2$, and $CH_4$). This suggests that the pore size for the membrane in Fig. S7c is between 2.89 Å and 3.3 Å[7].

## 6. Comparison to Modeling Results and Effusion

Jiang et al. simulated transport for two types of pores, a N-terminated one with a ~3 Å size and an H-terminated one with a ~2.5 Å size[8]. Their nominal $H_2$ permeance of 1 mol $m^{-2}$ $s^{-1}$ $Pa^{-1}$ was based on the N-terminated pore at 600 K with a pass through frequency of $10^{11}$ $s^{-1}$ where a 1 bar pressure drop was estimated from their simulation. When discussing the H-terminated (2.5 Å) pore at room temperature Jiang et al states that for $H_2$ the "passing-through frequency" is $10^9$ $s^{-1}$. This "passing-through frequency" is lower than the N-terminated by approximately two orders of magnitude for room temperature operation. Thus, we start with 1 mol $m^{-2}$ $s^{-1}$ $Pa^{-1}$ at 600 K and lower it to $10^{-2}$ mol $m^{-2}$ $s^{-1}$ $Pa^{-1}$ to accommodate the fact that our measurements were at room temperature. Then we multiply by the area that Jiang et al. used, which was 187 $Å^2$ (1.87 x $10^{-18}$ $m^2$), to arrive at ~$10^{-20}$ mol $s^{-1}$ $Pa^{-1}$.

To compare to selectivities predicted by the classical effusion model we plotted the leak rate for $H_2$ and $CO_2$ for membrane 'Bi- 3.4 Å' and $H_2$, $CO_2$, $N_2$, and $CH_4$ for membrane 'Bi- 4.9 Å' and included this in Figure S8 which is a plot of the normalized leak rate versus the inverse square root of the molecular mass of each gas species. Classical effusion predicts that the flow rate through a pore would scale with the inverse

square root of the molecular mass and therefore would monotonically increase with increasing inverse square root of the molecular mass. We can also compare the selectivity of $H_2$ to $CO_2$ for both membranes. For classical effusion the selectivity is the ratio of the square root of the molecular masses which is 4.7 for the case of $H_2$ to $CO_2$. For membranes 'Bi- 3.4 Å' and 'Bi- 4.9 Å' presented in Fig S8 the $H_2$ to $CO_2$ selectivities are 1.7 and 3 respectively. Tables S1, S2, and S3 show the ideal selectivity for 'Bi- 3.4 Å', 'Bi- 4.9 Å', and 'Mono- 5 Å', respectively. This suggests that we are not in the classical effusion regime. Classical effusion requires the pore size to be smaller than the mean free path of the molecule which is ~60 nm at room temperature and ambient pressures. However, we are in a regime where the pore size is much smaller and on the order of the molecule size, therefore it is necessary to consider the molecular size and chemistry.

## 7. Air leaking back into Microcavity

Figure S9 shows air leaking back into a microcavity after all the $H_2$ had rapidly escaped after etching. This is a bilayer sample that was etched in the same manner as the membranes presented in the main text. After etching the sample was filled with 200 kPa of $H_2$ before being imaged. Hydrogen quickly leaks out leaving a near vacuum in the microcavity under the graphene. After 3000 min the deflections changed from -90 nm to -50 nm. This leak rate is consistent with previously measured leak rates for air leaking into an initially evacuated microcavity of similar geometry[3]. This result further suggests that we are measuring the transport thorough the porous graphene for $H_2$ while $N_2$ is diffusing through the silicon oxide substrate.

**Supplementary References:**


1. Koh, Y.K., Bae, M.-H., Cahill, D.G. & Pop, E. Reliably counting atomic planes of few-layer graphene (n > 4). *ACS Nano* **5**, 269-274 (2011).

2. Reif, F. *Fundamentals of Statistical and Thermal Physics*. 651 (McGraw-Hill Book Company: New York, NY, 1965).

3. Bunch, J.S. *et al.* Impermeable atomic membranes from graphene sheets. *Nano Lett.* **8**, 2458-2462 (2008).

4. Hencky, H. Uber den spannungzustand in kreisrunden platten mit verschwindender

biegungssteiflgeit. *Z. fur Mathematik und Physik* **63**, 311-317 (1915).

5. Koenig, S.P., Boddeti, N.G., Dunn, M.L. & Bunch, J.S. Ultrastrong adhesion of graphene membranes. *Nature Nanotech.* **6**, 543-546 (2011).

6. Timoshenko, S., Young, D.H. & Weaver, W. *Vibration Problems in Engineering*. 481-484 (John Wiley and Sons, Inc.: New York, 1974).

7. Breck, D.W. *Zeolites Molecular Sieves: Structure, Chemistry, and Use*. 593-724 (Wiley: New York, NY, 1973).

8. Jiang, D.-en, Cooper, V.R. & Dai, S. Porous graphene as the ultimate membrane for gas separation. *Nano Lett.* **9**, 4019-4024 (2009).

**Supplementary Figures:**

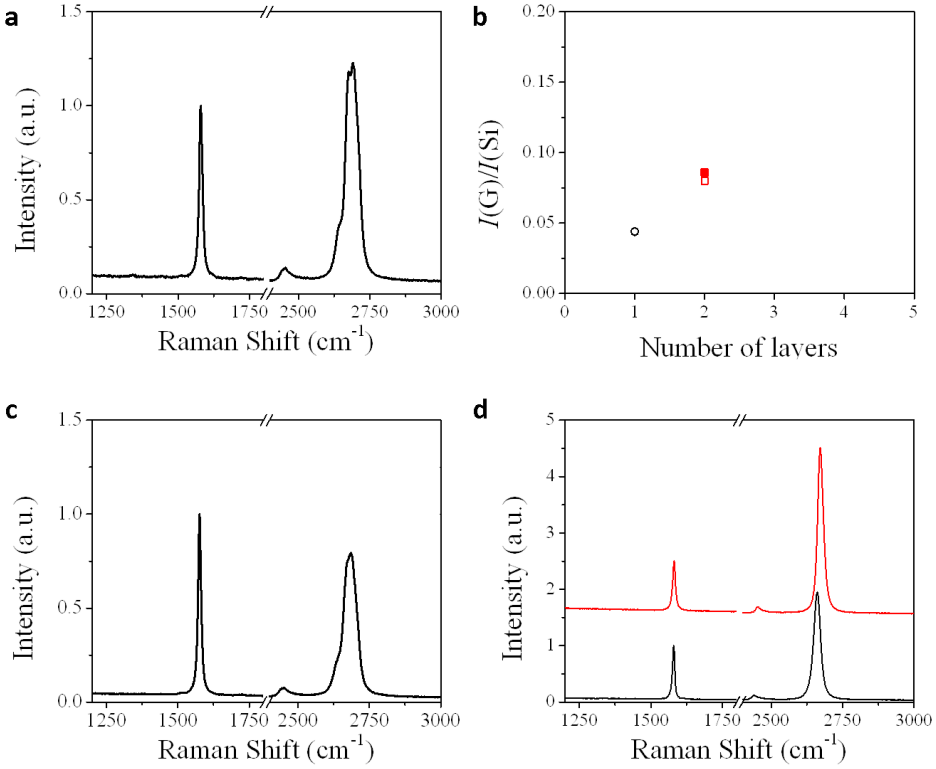


**Figure S1: Raman Spectrum of Graphene Samples**

**(a)** Raman spectrum of graphene flake containing membrane 'Bi- 3.4 Å' from the main text taken before etching.

**(b)** *I*(G)/*I*(Si) for flake in (a). The open circle and square were taken from a nearby flake containing both mono and bilayer sections.

**(c)** Raman spectrum of membrane 'Bi- 4.9 Å' from the main text before etching.

**(d)** Raman spectrum for the monolayer samples presented in the supplementary information. Upper red curve is from the flake containing 'Mono- 3.4 Å' from Figure S5 of the supplementary information after etching. The lower black curve is for the monolayer membrane presented in Figure S6. Both were taken after etching.

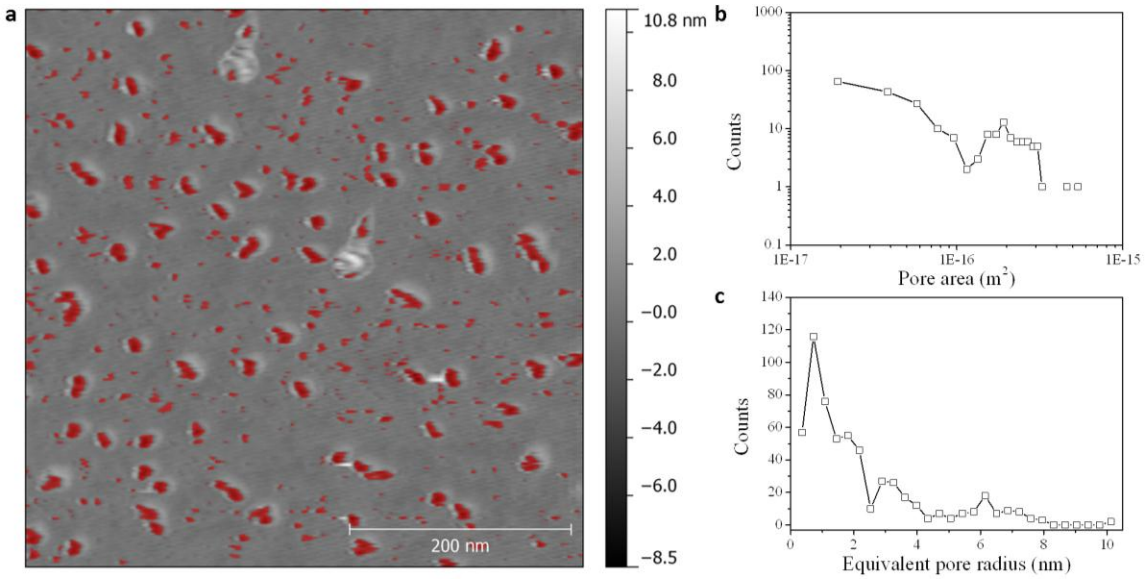


**Figure S2: Visualization of UV etching on suspended graphene**

**(a)** AFM scan of a membrane etched for a longer time to visualize the pore growth. The red areas are pits created by the UV etching.

**(b)** Histogram of the number of pores versus the approximate pore area.

**(c)** Histogram of the number of pores versus the equivalent radius of the pore. **(b)** and **(c)** indicate a nucleation and growth mechanism for pore evolution.

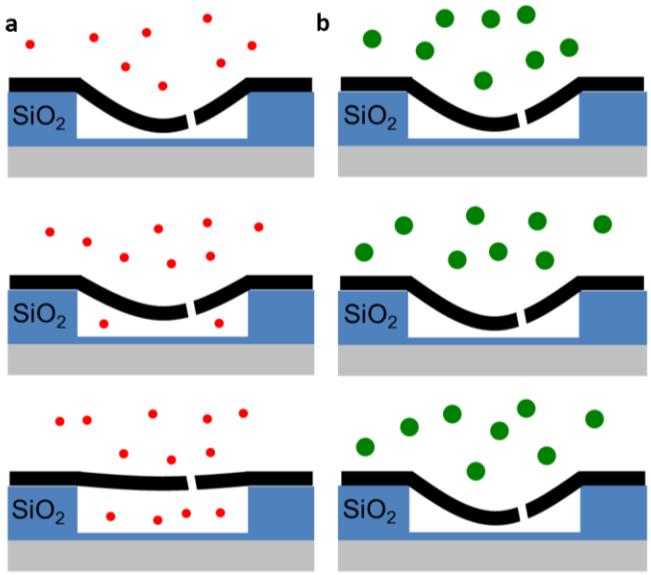


**Figure S3: Schematic of Resonant Frequency Leak Rate Measurements**

**(a)** Schematic of the gas permeation through porous graphene membranes as measured by optical resonance. First the membrane is put in vacuum and the membrane is flat with a frequency of $f_o$ corresponding to zero tension in the membrane. After a pressure of a given gas species is introduced to the vacuum chamber the pressure difference across the membrane will induce tension causing the vibrational frequency to increase. If the gas species kinetic diameter is smaller than that of the pore size (red) it will pass through the pore(s) and the pressure difference will equalize and, therefore, the tension and resonant frequency will decrease with time.

**(b)** If the gas species is larger than the pore size (green), the gas will not pass through the graphene membrane and the tension and resonant frequency will stay constant with time.

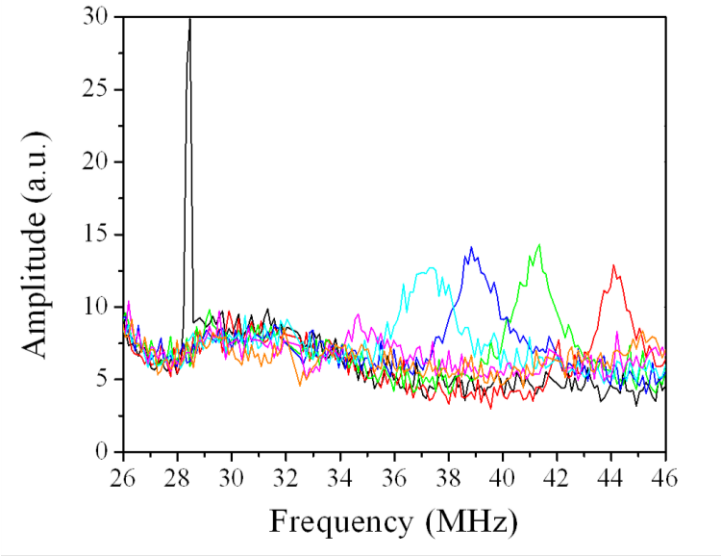


**Figure S4: Sample Resonant frequency curves for $CH_4$**

Amplitude vs drive frequency for 80 torr of $CH_4$. The data corresponds to the frequencies shown in Fig 3 inlay of main text taken at $t$ = 0 s (black), $t$ = 1 s (red), $t$ = 3 s (green), $t$ = 5 s (blue), $t$ = 7 s (cyan), $t$ = 11 s (magenta), and $t$ = 13 s (orange).

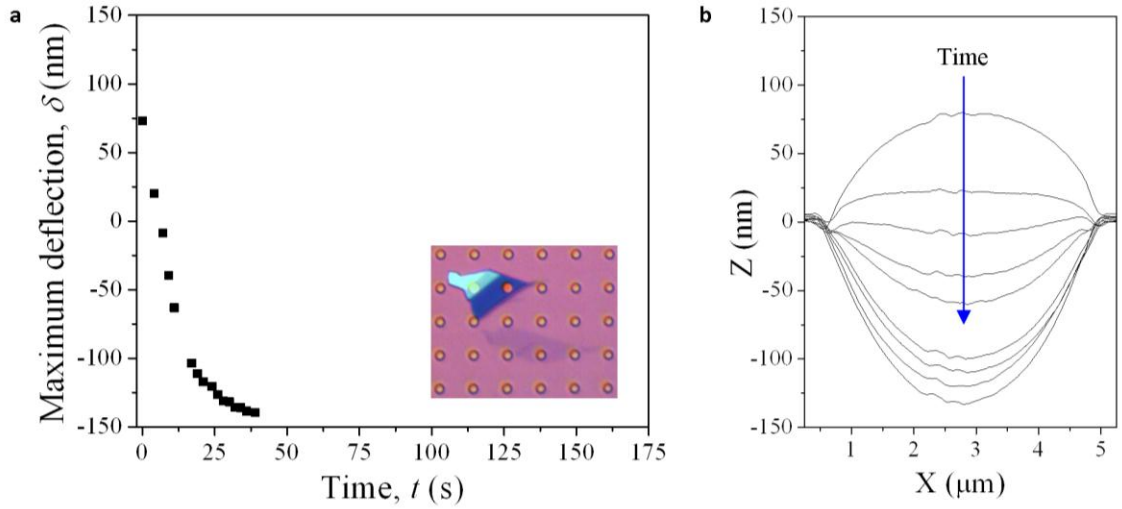


**Figure S5: Monolayer graphene showing selectivity $H_2/N_2$ selectivity**

**(a)** Maximum deflection, $\delta$, vs, $t$ for a monolayer membrane. The rapid decrease in deflection that becomes negative is consistent with the results seen in Fig 1 of the main text. Inlay: optical image of the monolayer graphene membrane covering one well in the substrate.

**(b)** AFM line scans of the membrane in (a) as time passes.

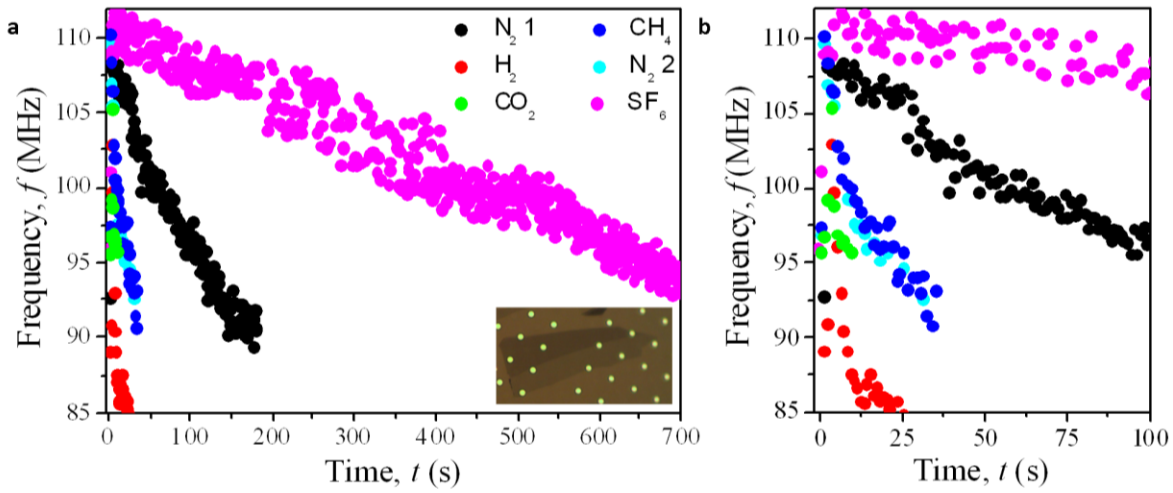


**Figure S6: Monolayer graphene showing $SF_6$ permeation and pore instability**

**(a)** Frequency vs time for $N_2$, $H_2$, $CO_2$, $N_2$, $CH_4$, and $SF_6$, taken in that order.

**(b)** A zoom in of (a). The change in $N_2$ leak rate indicates that the pore(s) in monolayer graphene are not stable and the pore size can change. After the pore was enlarged, the membrane was able to allow $SF_6$ to leak through the membrane.

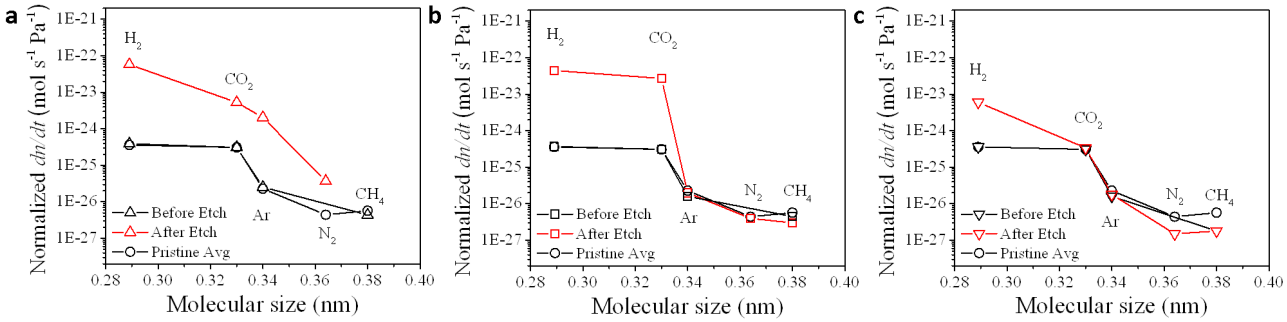


**Figure S7: Additional bilayer membranes measured**

**(a)** Normalized *dn*/*dt* vs. Molecular size showing permeation of all gas species larger than $CH_4$ before and after etching. This membrane was damaged before the $CH_4$ data could be taken.

**(b)** Normalized *dn*/*dt* vs. Molecular size for the membrane 'Bi-3.4 Å' before and after etching.

**(c)** Normalized *dn*/*dt* vs. Molecular size for a membrane showing an increase in the leak rate of $H_2$, and no significant increase in the leak rate for $CO_2$, Ar, $N_2$, and $CH_4$. **(a)**, **(b)**, and **(c)** where all from the same graphene flake that can be found in the inlay of Fig 1f.

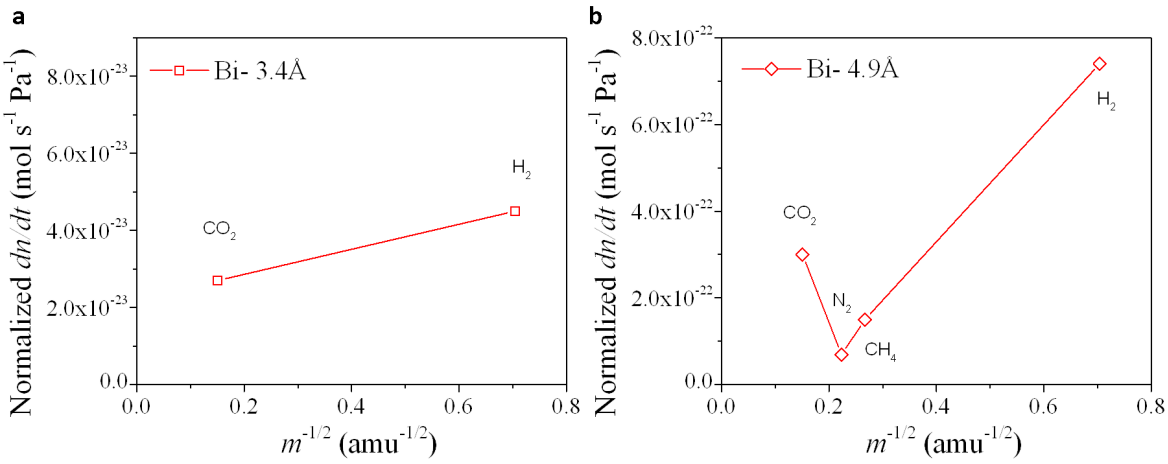


**Figure S8: Comparing Flow Rates to Classical Effusion**

**(a)** Normalized *dn/dt* for membrane 'Bi- 3.4 Å' plotted versus the inverse square root of the molecular mass of $H_2$ and $CO_2$.

**(b)** Normalized *dn/dt* for membrane 'Bi- 4.9 Å' plotted versus the inverse square root of the molecular mass of $H_2$, $CO_2$, $N_2$ and $CH_4$.

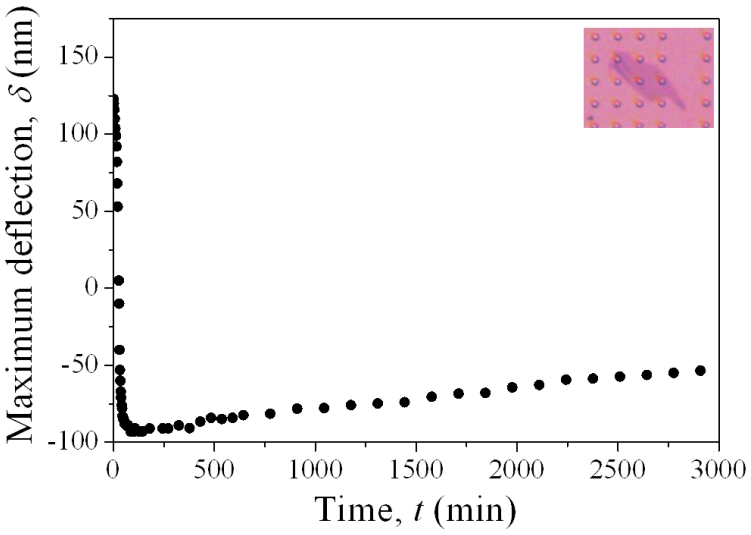


**Figure S9: Air leaking back into Microcavity**

Maximum deflection, $\delta$, vs, $t$ showing the air leaking back into the microcavity after all the $H_2$ has rapidly leaked out through pores created in the graphene. The microcavity was initially filled with 200 kPa of $H_2$. Inlay show the optical image of this sample.

**Supplementary Tables:**

**Table S1: Ideal gas separation factors for membrane 'Bi- 3.4 Å'**

| | $H_2$ | $CO_2$ | Ar | $N_2$ | $CH_4$ |
|---|---|---|---|---|---|
| $H_2$ | -- | 1.7 | $2x10^3$ | $10^4$ | $10^4$ |
| $CO_2$ | -- | -- | $5x10^2$ | $7x10^3$ | $9x10^3$ |
| Ar | -- | -- | -- | 5 | 7 |
| $N_2$ | -- | -- | -- | -- | 1.3 |
| $CH_4$ | -- | -- | -- | -- | -- |

**Table S2: Ideal gas separation factors for membrane 'Bi- 4.9 Å'**

| | $H_2$ | $CO_2$ | $N_2$ | $CH_4$ | $SF_6$ |
|---|---|---|---|---|---|
| $H_2$ | -- | 3 | 11 | 5 | N/A |
| $CO_2$ | -- | -- | 3.6 | 1.7 | N/A |
| $N_2$ | -- | -- | -- | 0.5 | N/A |
| $CH_4$ | -- | -- | -- | -- | N/A |
| $SF_6$ | -- | -- | -- | -- | -- |

**Table S3. Ideal gas separation factors from membrane 'Mono- 5 Å'**

| | $H_2$ | $CO_2$ | $N_2$ | $CH_4$ | $SF_6$ |
|---|---|---|---|---|---|
| $H_2$ | -- | 0.49 | 1.97 | 2.37 | 126 |
| $CO_2$ | -- | -- | 3.95 | 4.89 | 260 |
| $N_2$ | -- | -- | -- | 1.23 | 65.7 |
| $CH_4$ | -- | -- | -- | -- | 53.1 |
| $SF_6$ | -- | -- | -- | -- | -- |